Influence of Topography and Permafrost Condition on Changes in Arctic Water Storage

By

Nicholas Wondolowski

Bachelor of Science, Salem State University, 2016

Submitted to the Graduate Faculty of

the Dietrich School of Arts and Sciences in partial fulfillment

of the requirements for the degree of

Master of Science

University of Pittsburgh

2020

UNIVERSITY OF PITTSBURGH

DIETRICH SCHOOL OF ARTS AND SCIENCES

This thesis was presented

By

Nicholas Wondolowski

It was defended on

11/18/2020

and approved by

Mark Abbot, PhD, Professor, Committee Member

Joseph Werne, PhD, Professor, Committee Member

Eitan Shelef,,P.hD, Assistant Professor, Committee Chair

Influence of Topography and Permafrost Condition on Changes in Arctic Water Storage

Nicholas Wondolowski, MA

University of Pittsburgh, 2020

Widespread permafrost thaw across the Arctic can impact the global carbon budget and climate, alter the arctic ecosystem, and affect water fluxes into Arctic rivers and oceans. These effects are influenced by interactions among the hydrologic system, permafrost, climate, and topography, yet the influence of these interactions on large scale hydrologic responses to thaw remain largely unquantified. This study builds on a simple conceptual model to explore the correlation between thaw-related climatic parameters and changes in water storage (as observed by GRACE mass anomaly data) between 2002-2017, and then evaluates the influence of topography and permafrost condition on these relations. Our results, based on a multivariate linear regression (MLR) and partial correlation over an annual time scale, show that in areas of continuous permafrost, loss of water storage is more strongly correlated with increased snow depth than with increased air temperature. Correlation between snow depth and water storage weaken as permafrost coverage decreases, while the correlation between air temperature and water storage do not meaningfully change with permafrost cover. We also show that, compared to areas of partial permafrost cover, areas of continuous permafrost are associated with higher likelihood of negative correlation between snow depth and water storage, and that this likelihood also increases with hillslope-scale topographic gradient. These findings suggest that permafrost thaw in areas of continuous permafrost and high topographic gradient facilitate lateral drainage of water stores and permafrost meltwater to the riverine system, resulting in decreased local water storage over an annual time scale. In areas of flat terrain and/or partial permafrost cover these affects are less pronounced, likely due to lower gradient of the water table and/or a longer water residence time that stems from connection with sub-permafrost aquifers. These results highlight the importance of lateral subsurface and surface flows at the hillslope scale on large scale patterns of hydrologic response to permafrost thaw.

Table of Contents

List of Figures

1.0 Introduction

Permafrost regions cover 24% of the terrestrial northern hemisphere (Zhang et al., 2008). Widespread permafrost thaw driven by changes in climate can substantially alter local hydrology, topography, and ecology (Jorgenson and Osterkamp, 2005; Rowland et al., 2010) and influence global climate through the release of greenhouse gasses (Zimov et al., 2006; Schurr et al., 2008). These local and global impacts are strongly influenced by the hydrologic system and its feedbacks with permafrost thaw. For example, permafrost thaw can increase the subsurface hydrologic connectivity between taliks, aquifers, and surface water stores (streams, bogs, and lakes) (Kurylyk et al., 2014) and cause higher drainage efficiency. Changes to this efficiency can influence advective and conductive heat transport that influence permafrost thaw (Loranty et al., 2018) and active layer thickness (ALT -the thickness of the seasonally thawed soil), and also influence soil saturation and thus the rate of CO_2 and CH_4 emission from decomposition of soil organic material (Christensen et al., 2000; Treat et al., 2018). Increased drainage efficiency can also enhance river discharge, which may amplify fluvial erosion rates, and enhance sediment and freshwater supply to Arctic Oceans (Olefeldt et al., 2016; Gruber and Haeberli, 2007; Schaefer et al., 2011; Syvitski et al., 2002; Rawlins et al., 2009). These multipronged influences highlight the importance of hydrological processes on the response of the Arctic permafrost regions to changes in climate.

Changes in climate influence soil temperature and thus the rate and extent of permafrost thaw (Osterkamp et al., 2007; Jorgenson et al., 2006; Koven et al 2013) and the hydrology of permafrost areas. High air temperature can increase soil temperatures, and permafrost thaw is often modeled as a function of the square root of thaw index (cumulative number of degree-days above 0 ºC over a year) (Romanovsky and Osterkamp 1997, Peng et al., 2018). Soil temperatures are also influenced by winter air temperatures, and thus snow cover that insulates the soil can amplify permafrost warming and thaw in the subsequent summer (Stieglitz et al., 2003, Jorgenson et al., 2010, Parks et al., 2014). Given that permafrost is typically associated with low hydrologic permeability (Painter et al., 2013, Walvoord et al., 2012, Evans et al., 2020), these climatic factors are expected to influence hydrologic connectivity and thus surface and subsurface water storage (Walvoord et al., 2012, 2016, Andersen et al., 2020, Evans et al., 2020). However, snow depth, air temperature, and seasonality may have competing effects on permafrost thaw, (e.g., snow depth and snow-season length tend to be positively correlated, but have opposing effects on soil temperature, Lawrence and Slater., 2009, McGuire et al., 2016), and thus their integrated influence on hydrologic connectivity and water storage depends on the balance between these effects.

Hydrologic responses to permafrost thaw depend on variations in parameters such as topographic gradient and/or the continuity of permafrost cover (Fig. 1). Whereas spatially continuous permafrost typically confines water storage and mobility to the active layer (Walvoord et al., 2012, 2016, O'Connor et al., 2019, Andersen et al., 2020), spatially discontinuous permafrost facilitates hydrologic connectivity with deeper, subpermafrost aquifers and thus may enhance hydrologic circulation and residence time (Walvoord et al., 2012, McKenzie et al., 2020, Evans et al., 2020). Topographic gradient can influence surface and subsurface flows given that the spatial gradient in water head, which drives subsurface flows, often follows surface elevation (Beven and Kirkby 1979, Kane et al., 1991,

Walvoord et al., 2012). Changes in water storage and fluxes in response to permafrost thaw are likely to also be influenced by local factors such as vegetation, soil characteristics, lakes, and fire history (O'Connor et al., 2019, Koch et al., 2014). Whereas recent local-scale field and modeling efforts appreciably unraveled the hydrological influences of such factors (Koch et al., 2014, Evans 2017, 2020, O'Connor et al., 2019, Atchley et al., 2016, Andersen et al., 2020), the influences of parameters such as topography and permafrost cover on large scale hydrologic response to thaw remain largely unquantified.

Large scale changes in total water storage (combined soil moisture, ground water, surface water and snow water equivalent) are captured by the Gravity Recovery Anomaly Climate Experiment (GRACE) observations. GRACE observations are available with varying levels of post-processing ranging in resolutions from 0.5-1.0 degree (e.g., Chen et al., 2016), whereby gravity anomaly signals are converted to changes of water equivalent height (Rodell and Famiglietti, 1999). GRACE observations have been applied to explore temporal variations in ground and surface water that are potentially related to changes in permafrost conditions over large-scale Arctic watersheds (Vey et al., 2012; Im et al., 2015; Muskett et al., 2011; Muskett et al., 2009). Temporal increase in total water storage anomalies (TWSA) have been attributed to the formation and growth of hydrologically isolated taliks and lakes, where the thaw of ground ice, together with the density difference between water and ice, surface subsidence, and lake formation, result in increased water storage (Muskett et al., 2011; Muskett et al., 2009; Wang et al., 2015). Conversely, temporal decrease in water storage has also been attributed to talik growth, because such growth can increase the hydrologic-connectivity between taliks and facilitates drainage of previously isolated water bodies such as perched lakes and aquifers (Velicogna et al., 2012; Im et al., 2015; Muskett et al., 2011; Muskett et al., 2009; Chao et al., 2011). Thus, it appears that permafrost thaw can cause both a decrease or increase in water storage, and systematic patterns of large-scale changes in water storage in response to thaw remain elusive.

In this study we explore the influence of climate, permafrost condition, and topography on changes in water storage across the Arctic through a grid-based analysis of GRACE data, guided by a simple conceptual model (Fig. 1). This model conceptualizes how changes in water storage in response to permafrost thaw vary with topographic gradient and permafrost cover. Based on this model, the lateral flow of water from previously isolated water stores (i.e., lakes, taliks, permafrost meltwater) into the riverine system (Muskett et al., 2011), is higher in regions of high topographic gradient and continuous permafrost compared to regions of low topographic gradient and/or discontinuous permafrost (Walvoord et al., 2016). To explore the predictions of this conceptual model, we first compare the influence of climatic parameters (primarily snow thickness and air temperature) on August TWSA ($TWSA_{aug}$) using multivariate regression. We then calculate the probability of having significant correlation between the more influential climate parameter and $TWSA_{aug}$ in areas of different permafrost cover and topographic gradient.

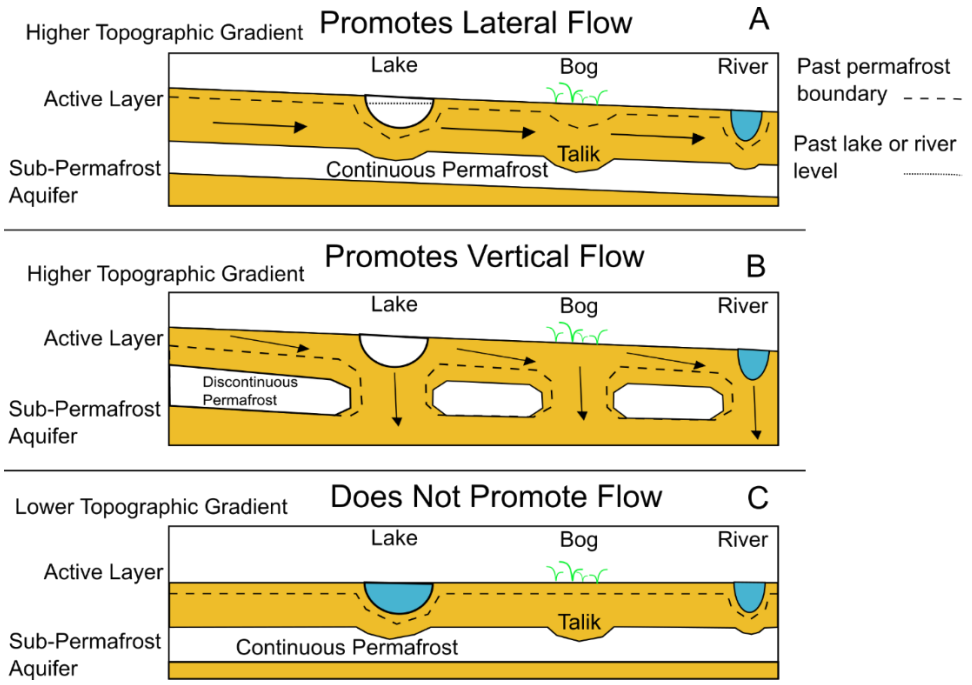

Figure 1. A Conceptual model showing the hydrologic response to permafrost thaw in three permafrost and topographic settings. Dashed line marks the pre thaw permafrost extent, and arrows indicate water flow directions. (A) Permafrost thaw in areas of considerable topographic gradient and continuous permafrost promote lateral drainage of water that used to be stored in/on the landscape prior to thaw. The increased hydrologic connectivity caused by permafrost thaw can drain lakes, taliks and permafrost meltwater into rivers that rapidly carry the water downstream, resulting in high likelihood for decreased water storage on annual time scales. (B) A similar setting to panel A, but underlain by discontinuous permafrost, can result in vertical drainage of water to sub-permafrost aquifers, where high storage space and residence time can result in a lower likelihood for decreased water storage over annual time scales, compared to areas of continuous permafrost (i.e., panel A). (C) A similar setting to panel A, but with lower topographic gradient that can inhibit lateral drainage due to low spatial gradient in water head, resulting in lower likelihood for decreased water storage in response to thaw compared to areas of high topographic gradient (i.e., panel A).

2.0 Methods

2.1 Study area and data

We studied land area north of 45 degrees latitude, excluding aquifers and areas within (2 GRACE pixel buffer) glaciated areas and coast lines (Fig. 3; GLIMS Glacial dataset). Water storage anomaly measurements rely on GRACE Level 3 global mascon hydrology data processed at NASA's Jet Propulsion Laboratory (Watkins et al., 2015; Wiese et al., 2016, 2018; Landerer et al., 2020). These data consist of globally gridded (0.5 degree) monthly mass measurements taken from 2002 to 2017 (Wiese et al., 2018, 2016; Watkins et al., 2015). Scaled uncertainty estimates for each mascon are reported with the original data. This data is interpreted to represent TWSA, and therefore is reported as water depth (cm) anomalies relative to a 2004 to 2009 mean. GRACE data were linearly interpolated to the 15th of August (when permafrost thaw and active layer thickness is assumed to be close to their annual maximum), with the exception of 2013 which is missing August and September data, producing a time series of August water storage anomalies ($TWSA_{aug}$).

Snow depth values were extracted from the Canadian Meteorological Centre data (Brown et al., 2010). The data consist of globally gridded (0.3 degrees) daily snow depth estimates from 1998 to 2017, derived from daily *in situ* snow depth measurements and interpolated using a snow accumulation and melt model in conjunction with a forecast model (Brown et al., 2010). Snow depth estimates are reported as snow water equivalent (SWE) using mean snow density observations at generalized Arctic snow-climate classes (e.g. alpine, tundra, prairie) (Sturm et al., 1995). Daily data were averaged to produce monthly SWE data for the 15th of each month and interpolated to GRACE resolution, while annual SWE represents the total monthly SWE.

Thaw index (TI, cumulative monthly temperatures greater than 0°C) was calculated from Global Historical Climatology Network version 2 and the Climate Anomaly Monitoring System (GHCN and CAMS) temperature dataset which consists of globally gridded (0.5 degree) mean monthly temperature estimates from 1948 to 2018. We computed TI for a mid-August to mid-August period, to match GRACE's mid-August observations. Monthly temperatures greater than 0°C were summed, and August temperature values were divided by 2 to approximate a mid-August value.

Precipitation values were extracted from the Climatic Research Unit Time Series v. 4.04 (Harris et al., 2020). The data consist of globally gridded (0.5 degree) monthly precipitation estimates derived from angular-distance weight interpolation of global weather station data (Harris et al., 2020). Mid-August to mid-August annual precipitation values were calculated by summing monthly precipitation between August 15th in consecutive years. As monthly data did not have mid-month intervals each August value was divided by 2 to approximate a mid-August value.

Evapotranspiration (ET) values were extracted from the Global Land Evapotranspiration Amsterdam Model Version 3 (GLEAM, Martens et al., 2017; Miralles et al., 2011). This data product consists of globally gridded (0.25 degree)

daily ET calculated from the Priestly and Taylor equation using satellite observed radiation and near-surface temperature (Miralles et al., 2011). GLEAM daily ET values were interpolated to GRACE resolution. Daily values were summed to produce mid-August to mid-August annual ET values.

Topographic data is based on the GTOPO30 dataset, a globally gridded 30-arc-second elevation data product created from various raster and vector elevation datasets by the U.S. Geological Survey (USGS). GTOPO30 was resampled in ArcGIS to pixels of equal size (1 x 1 km) to allow accurate calculation of topographic gradient (G) at the scale of Arctic hillslopes (McNamara et al., 1999; Crawford and Stanley, 2014):

$$G = \sqrt{(dz/dx)^2 + (dz/dy)^2} \qquad (1)$$

where dz/dx and dz/dy are the change in elevation in the x and y direction, respectively. The average gradient of all pixels within each GRACE pixel was then calculated to approximate a representative topographic gradient for each GRACE pixel.

Glacier and aquifer regions from the Global Land Ice Measurements from Space (GLIMS) and a global reservoir dataset, respectively, which lie in GRACE pixels were excluded from the analysis, as well as a buffer zone of two GRACE pixels around these pixels.

Permafrost categories were extracted based on a Circum-Arctic Map of Permafrost and Ground-Ice Conditions of 12.5km resolution (Brown et al., 2002). The resolution of the map was coarsened to GRACE resolution (0.5 x 0.5 degrees) based on the majority of values in each pixel.

2.2 The relative influence of TI and SWE on $TWSA_{aug}$

To estimate the influence of TI and SWE on $TWSA_{aug}$ we used a multivariate least square linear regression for each GRACE pixel in the area north of 45 degrees latitude using August to August data from 2002 to 2017. Precipitation and evapotranspiration were also included in the regression to account for their potential influence on $TWSA_{aug}$. To facilitate comparison of regression coefficients we also computed regression over z-scored values of the four independent parameters (i.e., $\sqrt{TI}$, SWE, Precipitation, Evapotranspiration). We tested the residuals for normality using Jarque–Bera Test (α=0.05), and for collinearity using a variance inflation factor (VIF). We identified all the pixels where the regression model was statistically significant (i.e., regression F-test with α=0.05) and with low collinearity (maximal VIF value<5), and computed regression coefficients and their p-value. Note that given the temporal variation in the uncertainty of $TWSA_{aug}$ (i.e., heteroscedasticity) the results only provide a general approximation. The strongest relation we identified (SWE- $TWSA_{aug}$) was explored further using methods defined in later sections.

2.3 Locations of significant SWE- $TWSA_{aug}$ correlation

We used partial correlation, combined with a Monte-Carlo simulation to further explore the relations between SWE and $TWSA_{aug}$. Partial correlation performed over multiple Monte-Carlo iterations can account for the influence of covariates and for the heteroscedasticity in the reported uncertainty for $TWSA_{aug}$. For each GRACE pixel, we computed a correlation coefficient (ρ) and p-value for the SWE- $TWSA_{aug}$ relations through a partial correlation procedure (Guilford J. P. and Fruchter B. 1973) that removes the influence of precipitation and evapotranspiration. To account for the heteroskedasticity in $TWSA_{aug}$, we repeated this procedure 100 times, where in each iteration the $TWSA_{aug}$ value was randomly selected from a gaussian distribution centered on the reported $TWSA_{aug}$ value, with a standard deviation that is based on the mascon scaled uncertainty estimates. We identified pixels as having statistically significant correlations between SWE and $TWSA_{aug}$ if: (a) At least 95% of these iterations produced partial-correlation p-values<0.05; (b) The maximal and minimal correlation coefficient (ρ) had the same sign. Given that clusters of GRACE pixels with significant statistical correlation are likely more reliable than isolated pixels we used morphologic opening to remove isolated pixels.

2.4 Permafrost categories, topographic gradient, and the occurrence of statistically significant SWE- $TWSA_{aug}$ correlation

To explore the influence of permafrost categories and topographic gradient on the occurrence of statistically significant positive and negative SWE- $TWSA_{aug}$ correlation, we computed the likelihood (P) of such occurrences in each permafrost or gradient category:

$$P = \frac{A_{st}}{A} \qquad (2)$$

The parameter $A_{st,}$ is the overall area [L^2] of pixels with significant SWE- $TWSA_{aug}$ correlations for a given permafrost or gradient category, and A is the total area of the associated permafrost or gradient category. Areas are computed while accounting for the change in GRACE pixel area with latitude. For each permafrost or gradient category, we computed P separately for positive and negative SWE- $TWSA_{aug}$ correlation. Permafrost categories were based on the standard classification to continuous, discontinuous, sporadic, and isolated (Brown et al., 2002). Gradient categories were defined by dividing the entire span of gradient values to discrete classes of equal range (0.006, based on the uncertainty of GTOPO30 elevation values).

3.0 Results

3.1 Multivariate regression results

The multivariate regression quantified the association between SWE and TI to $TWSA_{aug}$. The regression was statistically significant (α=0.05, F-test) for 11.6% of the GRACE pixels included in the analysis. The mean regression coefficients are shown in Figure 2 (i.e., the coefficients are averaged over all the pixels with statistically significant regression and their associated p-values and their uncertainties). The absolute value of the regression coefficient for z-scored variables was higher for SWE compared to TI in 85% of the pixels with statistically significant regression. The coefficient p-value was lower for SWE compared to TI in 84% of these pixels. These comparably higher coefficient values and lower p-values suggest that for the analyzed pixels $TWSA_{aug}$ is associated more strongly with SWE than with TI. The difference in influence of SWE and TI on TWSA (SWE having higher influence) decreases as permafrost extent decreases.

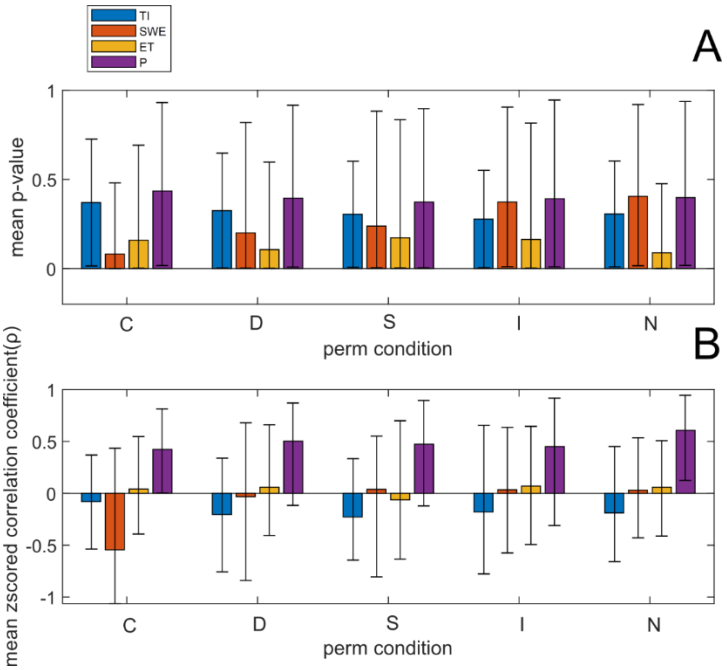

Figure 2. Bar plots showing multivariate linear regression results, including (A) p-value, (B) mean z-scored correlation coefficient between each of the explanatory variables and $TWSA_{aug}$, where C is continuous, D is discontinuous, S is sporadic, I is isolated, and N is non-permafrost. Error bars show 5 and 95 percentiles.

3. 2 Partial correlation results

We used partial correlation to identify locations where the correlation between SWE and $TWSA_{aug}$ is statistically significant while accounting for the influence of precipitation and ET. The partial correlation produced statistically significant correlation ($p<0.05$) for 5.1% of the analyzed GRACE pixels (Fig. 3a). Of these pixels 1.2% and 98.8% have positive and negative SWE- $TWSA_{aug}$ correlations, respectively. Pixels with positive and negative SWE-$TWSA_{aug}$ relations have ρ values of 0.71+/-0.04 and -0.82+/-0.06, respectively (uncertainty is reported as one standard deviation of all pixels with significant correlation).

.

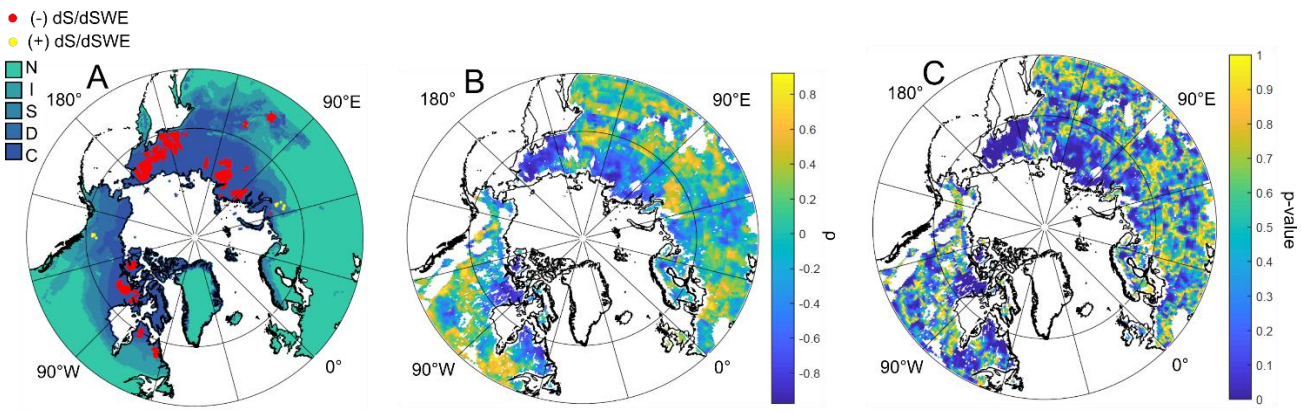

Figure 3. Circumpolar maps that show: (A) locations of significant SWE-$TWSA_{aug}$ correlation on top of permafrost cover map (Brown et al., 2002) where C is continuous, D is discontinuous, S is sporadic, I is isolated, and N is non-permafrost. (B, C) the mean correlation coefficient (ρ) and p-values for the partial correlation. White colored areas inside the black continental outlines were not considered in the analysis as they contain either aquifers, glaciers, or coastlines, and their associated buffer zones.

3. 3 Influence of permafrost on spatial distribution of significant SWE- $TWSA_{aug}$ pixels

We used a probabilistic approach (Equation 2) to quantify the influence of permafrost cover on the occurrence of significant correlation between SWE and $TWSA_{aug}$. Overall, there is a higher probability (P) of having significant SWE- $TWSA_{aug}$ correlation in permafrost (continuous, discontinuous, sporadic, and isolate) compared to non-permafrost pixels (0.106 vs 0.001, respectively, Fig. 4). Negative SWE-$TWSA_{aug}$ correlations were overwhelmingly more likely to occur in continuous permafrost (Fig. 4) compared to other permafrost categories, comprising 96% of all the pixels with significant SWE-$TWSA_{aug}$ correlation.

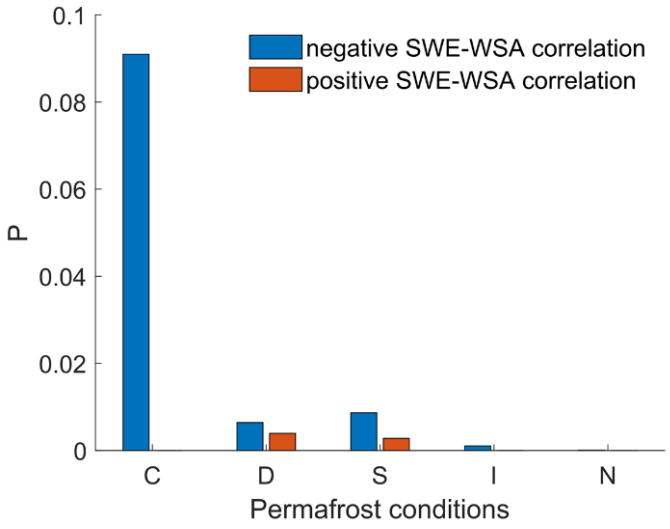

Figure 4. Probability of having significant SWE- $TWSA_{aug}$ correlation in varying permafrost conditions (i.e., Equation 2); where C is continuous, D is discontinuous, S if sporadic, I is isolated, and N is non-permafrost. Note that the likelihood of significant negative correlation is overwhelmingly more common in areas of continuous permafrost.

3.4 Influence of topographic gradient on spatial distribution of SWE- $TWSA_{aug}$ correlation

To explore the relations between topographic gradient and $TWSA_{aug}$ we analyzed the likelihood of having a statistically significant SWE- $TWSA_{aug}$ correlation as a function of topographic gradient. Only the continuous permafrost zone had a sufficient number of significant pixels for a robust analysis (i.e., n>10 pixels per topographic gradient category). We find that topographic gradient (G) positively correlates ($P=2.09G+0.10$, $R^2=0.61$, p-value=0.0004, Fig. 5) with the probability (P) of a pixel having a negative SWE- $TWSA_{aug}$ correlation. The number of pixels with significant positive SWE- $TWSA_{aug}$ correlation was too low to conduct a robust analysis for such correlation.

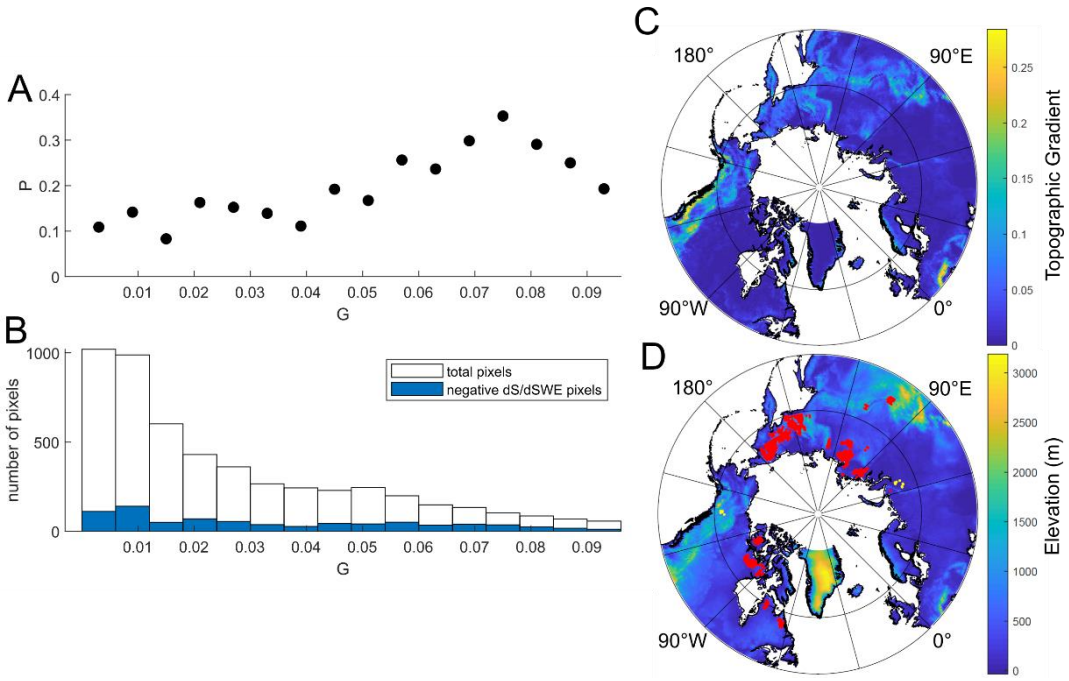

Figure 5. The influence of topographic gradient on changes in water storage. (A) the probability of having negative SWE- $TWSA_{aug}$ relations at different gradient categories (i.e., Equation 2). (B) the total number of pixels and the number of pixels with negative SWE- $TWSA_{aug}$ relations within each topographic gradient bin. (C) a map of topographic gradient (averaged over each grace pixel). (D) a map of elevation above sea level (averaged over each grace pixel) with location of pixels with significant SWE- $TWSA_{aug}$ correlation marked in red.

4.0 Discussion

4.1 SWE- $TWSA_{aug}$ correlation and permafrost thaw

The dominant negative correlation between SWE and $TWSA_{aug}$ in areas of continuous permafrost (Fig. 4) likely reflects the insulating effect of snow on soil temperature (Stieglitz et al., 2003, Lawrence et al., 2009; Park et al., 2014) and thus on the hydrologic properties of the soil. These negative relations also suggest that water inputs from increased SWE have drained by the following summer (Dornes et al., 2008), or that the remaining summer SWE is negligible compared to other hydrologic changes. High snow thickness is associated with higher winter soil temperatures (Park et al., 2014; Wang et al., 2017) which may extend the duration of active layer thaw (Park et al., 2014), and the ALT in the following summer (Lawrence et al., 2008; 2010, Parks et al., 2015). This likely influences the duration over which the active layer can conduct water, as well as the hydrologic transmissivity of the active layer (Jacques et al., 2009), resulting in a higher potential for water loss through lateral subsurface flow and drainage into the riverine system (Figure 1). The dominance of the negative correlation between SWE and $TWSA_{aug}$ suggests that despite the competing influences of high snow thickness and long winters on permafrost thaw (Lawrence and Slater 2010, McGuire et al., 2018), overall, a high SWE is associated with temporal and/or spatial expansion of thaw that increases hydrologic connectivity.

4.2 Mechanisms for water loss

Although the coarse spatial resolution of this study obscures the fine scale mechanisms of change in water storage, the association between changes in water storage, permafrost cover (Fig. 4) and topographic gradient (Fig. 5) support the mechanisms proposed by the conceptual model (Fig. 1). The association with continuous permafrost suggests that water loss stems primarily from supra-permafrost lateral flow (Walvoord et al., 2012, Scheidegger, 2013). A loss of water may reflect the lateral drainage of recently thawed permafrost meltwater, as well as of surface and subsurface water stores that were previously confined by permafrost. Such stores may include permafrost bound aquifers (Hinzman et al., 2006), closed and open taliks (Walvoord et al., 2016), water stores behind impermeable ice dams (Oconnor et al., 2018; Neilson et al., 2018) and permafrost bound lakes (Walvoord et al., 2016). The loss of permafrost confinement around these water stores likely stems from increased ALT and localized thaw, that cause increased connectivity of flow pathways along features such as ice-wedges (Woo et al., 2006, Liljedhal et al., 2016) or water tracks (McNamara et al., 1998, Rushlow and Godsey, 2017). The association of water loss with mean hillslope-scale topographic-gradient suggests that the loss of water occurs through hillslope-scale lateral flows whose rate is influenced by topographic gradient. This is consistent with standard models of surface and subsurface flows where the water head follows the surface topography (Beven and Kirkby 1979, Kane et al., 1991, Walvoord et al., 2012). These flows drain the hillslopes into the riverine system and may contribute to the observed increase in river discharge and baseflow across the Arctic (Jacques et al., 2009). The rapid flow rate within

the riverine system (e.g., 25-40 cm/s, O'Brien et al., 2001; Quinton and Marsh, 1998, Swenson et al., 2012) facilitates rapid drainage out of a GRACE pixel domain, resulting in the observed change in $TWSA_{aug}$ over the annual time scale of our analysis.

From a modeling perspective, the association between hillslope-scale topographic gradient and SWE -$TWSA_{aug}$ correlation highlights the importance of topographically driven lateral subsurface flow at the hillslope scale. Such flows are typically overlooked by large-scale Earth Systems Models (ESMs) (Lawrence et al., 2019; Oleson et al., 2013; Swenson et al., 2019), and thus our findings suggest that such models may miss an important component of Arctic hydrology. Further, given that the element size of such ESMs is typically similar to that of a GRACE pixel (Swenson et al., 2012), our findings point at the potential of GRACE-derived information to improve and validate such models.

4.3 Importance of permafrost condition

Locations of statistically significant negative correlation between SWE and $TWSA_{aug}$ primarily occur within areas of continuous permafrost cover (Fig. 4). The MLR results indicate high influence of SWE on $TWSA_{aug}$ with decreasing influence as permafrost extent decreases (Fig. 2), suggesting that SWE- $TWSA_{aug}$ relations depend on permafrost conditions. This aligns with the proposed conceptual model (Fig. 1), as regions with lesser permafrost coverage may already have higher connectivity between water stores and therefore may not experience a substantial change in $TWSA_{aug}$ in response to further permafrost thaw. The decrease in influence of SWE on TWSA with decreasing permafrost extent shown in the MLR results (Fig. 2) suggests that processes described in our conceptual model (Fig. 1) operate on a more continuous spectrum. In addition, connectivity between supra- and sub-permafrost aquifers enables vertical water flow (Walvoord et al., 2012, 2016, McKenzie et al., 2020, Evans et al., 2020) and likely increase the residence time of water within a GRACE pixel domain compared to areas of continuous permafrost where flows are primarily lateral (OCconor et al., 2018, Walvoord et al., 2012, Muskett and Romanovsky., 2011). Overall, these results suggest that the annual water-loss in response to changes in SWE increases with permafrost cover.

4.4 Comparison to past work

The spatial patterns identified through our analysis can help integrate the findings of prior GRACE studies with long term snow fall trends. The two clusters of significant SWE-$TWSA_{aug}$ correlation that we identified in north-central Siberia (73N 90E, 72N 113E, Fig. 3a) occur in areas of continuous permafrost that are associated with a decadal increase in water storage between 2003-2012 (Im et al., 2015) and a decrease in SWE between 1980-2018

(Pulliainen et al., 2020). This temporal decrease in SWE and increase in TWSA (i.e., Im et al., 2015) is consistent with the negative correlation we observe between SWE and $TWSA_{aug}$ in these regions. Such consistency also prevails over the Lena watershed, where GRACE- based studies show a temporal increase in water storage (Im et al., 2015; Muskett et al., 2009, 2011; Vey et al., 2012; Landerer et al., 2010), which is consistent with observations of a temporal decrease in SWE (Pulliainen et al., 2020) and the negative SWE-$TWSA_{aug}$ correlation we observed (Fig. 3b). In contrast, the Mackenzie and Yukon watersheds in North America are generally associated with a temporal decrease in both TWSA and SWE (Muskett et al., 2009, 2011; Pullianinen et al., 2020). The lack of negative SWE-TWSA relations in these basins is aligned with our results, as a large portion of these watersheds is not underlain by continuous permafrost (Figs 1-3). Whereas this integrated analysis generally supports our results, its validity is constrained by the temporal mismatch between the time scale of our observations (2002-2017), previous Arctic GRACE studies (2002-2013 or shorter), and the SWE data compilation (1980-2018, Pulliainen et al., 2020), as well as by the temporal fluctuation in climate over the duration of prior GRACE studies (e.g., Im et al., 2015, Vey et al., 2012).

An association between topographic gradient and changes in water storage measured by GRACE was explored by Im et al., (2015). Their findings show a positive correlation between topographic gradient and temporal increase in water storage (Im et al., 2015) over a decadal time scale (2003-2012) based on the representative gradient and TWSA characteristics of 11 zones in Central Siberia. They suggest that the relatively high sand and gravel content in high gradient areas enables more infiltration and increased water storage compared to low gradient areas where impermeable clays are more common. Whereas this may appear contradictory to our finding (i.e., a positive correlation between topographic gradient and the likelihood of having a negative SWE-$TWSA_{aug}$ over areas of continuous permafrost) these findings are not directly comparable. This is because the study of Im et al., 2015 and this study respectively explore different variables (i.e., time-TWSA and SWE-$TWSA_{aug}$), different time scales (decadal vs annual), different resolutions (11 zones vs. thousands of GRACE pixels), different areas (Central Siberia vs the entire Northern Circumpolar area), and different degrees of permafrost cover (a combination of permafrost cover categories vs. continuous permafrost only). Additionally, the interpretation of Im et al., (2015) emphasizes the potential influence of parameters, such as soil composition, that are not included in the simple conceptual model of Figure 1.

4.5 Future implications

Our results provide some insights regarding future changes to water storage. Generally speaking, Arctic snowfall magnitude is projected to decrease while variability is projected to increase in the coming decades (Zhong et al., 2018; Osuch et al., 2017; Bintanja et al., 2017, 2020; Pullianinen et al., 2019), while the duration of the snow fall season is expected to decrease due to continued increase in air temperature (Bintanja et al., 2017). A general trend towards shorter (promotes thaw) and less intense (does not promote thaw) snowfall seasons (as described above),

result in competing effects on permafrost thaw (Lawrence et al., 2009), making predictions of snow depth influence on Arctic water storage difficult. Regardless of snowdepth trends, our conceptual model (Fig. 1) is relevant to the influence of permafrost condition and topography on Arctic water storage during times of permafrost thaw, which is projected to continue (Jorgenson et al., 2010). Changes in Arctic water storage may influence the emissions of methane and carbon dioxide from thawed permafrost soils. These emissions depend, among other things, on the soil's oxygen conditions, where carbon dioxide is primarily emitted from dry aerobic soils, and methane emission is favored by saturated anaerobic soils (Christensen et al., 2000; Treat et al., 2016). The relatively large water loss from areas of high topographic gradient, continuous permafrost cover and thick winter snow cover, suggest that such areas are more likely to dry and emit a higher fraction of carbon dioxide relative to methane. Changes in subsurface hydrologic connectivity in response to future climate conditions may exacerbate this pattern.

5.0 Conclusions

Analysis of circumpolar GRACE data reveals relations between climate, permafrost condition, topography and hydrology that are consistent with a simple conceptual model. Our findings suggest that (1) the influence of SWE on annual changes in TWSAaug is larger than that of TI in areas of continuous permafrost cover, a difference which decreases with percent permafrost cover; (2) that a negative correlation between SWE and TWSAaug is more likely than a positive correlation and that this likelihood is particularly high in areas of continuous permafrost cover; (3) in areas of continuous permafrost, the likelihood of negative correlation between SWE and TWSAaug increases with topographic gradient. These findings suggest that the insulating effects of snow cover from cold winter air temperatures can increase subsurface connectivity between water stores and/or the duration of drainage. In areas of continuous permafrost and pronounced topographic gradient, the water drains laterally into the riverine system that can rapidly transport it out of a GRACE pixel domain, resulting in high likelihood for decreased water storage in response to increased SWE over an annual time scale. This likelihood is lower in areas of partial permafrost cover and/or low topographic gradient, where the residence time of water is likely longer. These results highlight the importance of hillslope scale lateral flows on circumpolar scale patterns of hydrologic response to permafrost thaw.

Bibliography

Andresen, C.G., Lawrence, D.M., Wilson, C.J., McGuire, A.D., Koven, C., Schaefer, K., Jafarov, E., Peng, S., Chen, X., Gouttevin, I. and Burke, E (2020). Soil moisture and hydrology projections of the permafrost region – a model intercomparison. *The Cryosphere, 14*(2), 445-459. doi:10.5194/tc-14-445-2020

Atchley, A. L., Coon, E. T., Painter, S. L., Harp, D. R., & Wilson, C. J. (2016). Influences and interactions of inundation, peat, and snow on active layer thickness. *Geophysical Research Letters, 43*(10), 5116-5123. doi:10.1002/2016gl068550

Beven, K. J., & Kirkby, M. J. (1979). A physically based, variable contributing area model of basin hydrology / Un modèle à base physique de zone d'appel variable de l'hydrologie du bassin versant. *Hydrological Sciences Bulletin, 24*(1), 43-69. doi:10.1080/02626667909491834

Bintanja, R., & Andry, O. (2017). Towards a rain-dominated Arctic. *Nature Climate Change, 7*(4), 263-267. doi:10.1038/nclimate3240

Blaen, P. J., Hannah, D. M., Brown, L. E., & Milner, A. M. (2014). Water source dynamics of high Arctic river basins. Hydrological processes, 28(10), 3521-3538.

Brown, R. D. and B. Brasnett. 2010, updated annually. Canadian Meteorological Centre (CMC) Daily Snow Depth Analysis Data, Version 1. [Indicate subset used]. Boulder, Colorado USA. NASA National Snow and Ice Data Center Distributed Active Archive Center. doi: https://doi.org/10.5067/W9FOYWH0EQZ3. [2020-01-15].

Chao, B. F., Wu, Y. H., Zhang, Z., & Ogawa, R. (2011). Gravity Variation in Siberia: GRACE Observation and Possible Causes. *Terrestrial, Atmospheric and Oceanic Sciences, 22*(2), 149-155. doi:10.3319/TAO.2010.07.26.03(TibXS)

Chen, Y., Li, W., Deng, H., Fang, G., & Li, Z. (2016). Changes in Central Asia's Water Tower: Past, Present and Future. *Sci Rep, 6*, 35458. doi:10.1038/srep35458

Christensen, T.R., Friborg, T., Sommerkorn, M., Kaplan, J., Illeris, L., Søgaard, H., Nordstrøm, C. and Jonasson, S., (2000). Trace gas exchange in a high-Arctic valley: 1. Variations in CO2 and CH4 Flux between tundra vegetation types. Global Biogeochemical Cycles, 14(3), 701-713.

Crawford, J. T., & Stanley, E. H. (2018). Distinct Fluvial Patterns of a Headwater Stream Network Underlain by Discontinuous Permafrost. *Arctic, Antarctic, and Alpine Research, 46*(2), 344-354. doi:10.1657/1938-4246-46.2.344

Dornes, P. F., Pomeroy, J. W., Pietroniro, A., Carey, S. K., & Quinton, W. L. (2010). Influence of landscape aggregation in modelling snow-cover ablation and snowmelt runoff in a sub-arctic mountainous environment. *Hydrological Sciences Journal, 53*(4), 725-740. doi:10.1623/hysj.53.4.725

Evans, S. G., & Ge, S. (2017). Contrasting hydrogeologic responses to warming in permafrost and seasonally frozen ground hillslopes. *Geophysical Research Letters*. doi:10.1002/2016gl072009

Evans, S. G., Yokeley, B., Stephens, C., & Brewer, B. (2020). Potential mechanistic causes of increased baseflow across northern Eurasia catchments underlain by permafrost. *Hydrological Processes*. doi:10.1002/hyp.13759

Evans, S. G., Yokeley, B., Stephens, C., & Brewer, B. (2020). Potential mechanistic causes of increased baseflow across northern Eurasia catchments underlain by permafrost. Hydrological Processes, 34(11), 2676-2690.

Gruber, S., & Haeberli, W. (2007). Permafrost in steep bedrock slopes and its temperature-related destabilization following climate change. *Journal of Geophysical Research, 112*(F2). doi:10.1029/2006jf000547

Guilford, J. P. (1950). Fundamental statistics in psychology and education.

Harris, I., Osborn, T. J., Jones, P., & Lister, D. (2020). Version 4 of the CRU TS monthly high-resolution gridded multivariate climate dataset. *Sci Data, 7*(1), 109. doi:10.1038/s41597-020-0453-3

Hinzman, L. D., & Kane, D. L. (1987). Active layer hydrology for Imnavait Creek, Toolik, Alaska (No. DOE/ER/60247-T2). Alaska Univ., Fairbanks, AK (United States). Water Research Center.

Im, S. T., & Kharuk, V. I. (2015). Dynamics of water mass in the Central Siberia permafrost zone based on gravity survey from the grace satellites. *Izvestiya, Atmospheric and Oceanic Physics, 51*(8), 806-818. doi:10.1134/s0001433815080046

Jorgenson, M. T., Shur, Y. L., & Pullman, E. R. (2006). Abrupt increase in permafrost degradation in Arctic Alaska. *Geophysical Research Letters, 33*(2). doi:10.1029/2005gl024960

Jorgenson, M.T., Romanovsky, V., Harden, J., Shur, Y., O'Donnell, J., Schuur, E.A., Kanevskiy, M. and Marchenko, S (2010). Resilience and vulnerability of permafrost to climate change. Canadian Journal of Forest Research, 40(7), 1219-1236.

Kane, D. L., Hinzman, L. D., Benson, C. S., & Liston, G. E. (1991b). Snow hydrology of a headwater Arctic basin: 1. Physical measurements and process studies. Water Resources Research, 27(6), 1099-1109.

Koch, J. C., Kikuchi, C. P., Wickland, K. P., & Schuster, P. (2014). Runoff sources and flow paths in a partially burned, upland boreal catchment underlain by permafrost. *Water Resources Research, 50*(10), 8141-8158. doi:10.1002/2014wr015586

Koven, C. D., Riley, W. J., & Stern, A. (2013). Analysis of permafrost thermal dynamics and response to climate change in the CMIP5 Earth System Models. Journal of Climate, 26(6), 1877-1900.

Kurylyk, B. L., MacQuarrie, K. T., & McKenzie, J. M. (2014). Climate change impacts on groundwater and soil temperatures in cold and temperate regions: Implications, mathematical theory, and emerging simulation tools. Earth-Science Reviews, 138, 313-334.

Landerer, F. W., Dickey, J. O., & Güntner, A. (2010). Terrestrial water budget of the Eurasian pan-Arctic from GRACE satellite measurements during 2003–2009. Journal of Geophysical Research: Atmospheres, 115(D23).

Landerer, F. W., Flechtner, F. M., Save, H., Webb, F. H., Bandikova, T., Bertiger, W. I., et al. (2020). Extending the global mass change data record: GRACE Follow-On instrument and science data performance. Geophysical Research Letters, 47, e2020GL088306. https://doi.org/10.1029/2020GL088306

Lawrence, D. M., Slater, A. G., Tomas, R. A., Holland, M. M., & Deser, C. (2008). Accelerated Arctic land warming and permafrost degradation during rapid sea ice loss. Geophysical Research Letters, 35(11).

Lawrence, D. M., & Slater, A. G. (2009). The contribution of snow condition trends to future ground climate. *Climate Dynamics, 34*(7-8), 969-981. doi:10.1007/s00382-009-0537-4

Lawrence, D.M., Fisher, R.A., Koven, C.D., Oleson, K.W., Swenson, S.C., Bonan, G., Collier, N., Ghimire, B., van Kampenhout, L., Kennedy, D. and Kluzek, E., (2019). The Community Land Model Version 5: Description of New Features, Benchmarking, and Impact of Forcing Uncertainty. *Journal of Advances in Modeling Earth Systems, 11*(12), 4245-4287. doi:10.1029/2018ms001583

Liljedahl, A.K., Boike, J., Daanen, R.P., Fedorov, A.N., Frost, G.V., Grosse, G., Hinzman, L.D., Iijma, Y., Jorgenson, J.C., Matveyeva, N. and Necsoiu, M. (2016). Pan-Arctic ice-wedge degradation in warming permafrost and its influence on tundra hydrology. *Nature Geoscience, 9*(4), 312-318. doi:10.1038/ngeo2674

Loranty, M.M., Abbott, B.W., Blok, D., Douglas, T.A., Epstein, H.E., Forbes, B.C., Jones, B.M., Kholodov, A.L., Kropp, H., Malhotra, A. and Mamet, S.D., (2018). Reviews and syntheses: Changing ecosystem influences on soil thermal regimes in northern high-latitude permafrost regions. *Biogeosciences, 15*(17), 5287-5313. doi:10.5194/bg-15-5287-2018

Luo, D., Wu, Q., Jin, H., Marchenko, S. S., Lü, L., & Gao, S. (2016). Recent changes in the active layer thickness across the northern hemisphere. *Environmental Earth Sciences, 75*(7). doi:10.1007/s12665-015-5229-2

Martens, B., Gonzalez Miralles, D., Lievens, H., Van Der Schalie, R., De Jeu, R.A., Fernández-Prieto, D., Beck, H.E., Dorigo, W. and Verhoest, N., (2017). GLEAM v3: satellite-based land evaporation and root-zone soil moisture. *Geoscientific Model Development, 10*(5), 1903-1925. doi:10.5194/gmd-10-1903-2017

McGuire, A.D., Koven, C., Lawrence, D.M., Clein, J.S., Xia, J., Beer, C., Burke, E., Chen, G., Chen, X., Delire, C. and Jafarov, E., (2016). Variability in the sensitivity among model simulations of permafrost and carbon dynamics in the permafrost region between 1960 and 2009. *Global Biogeochemical Cycles, 30*(7), 1015-1037. doi:10.1002/2016gb005405

McKenzie, J. M., Kurylyk, B. L., Walvoord, M. A., Bense, V. F., Fortier, D., Spence, C., & Grenier, C. doi:10.5194/tc-2020-132

McNamara, J. P., Kane, D. L., & Hinzman, L. D. (1998). An analysis of streamflow hydrology in the Kuparuk River Basin, Arctic Alaska: a nested watershed approach. Journal of Hydrology, 206(1-2), 39-57.

McNamara, J. P., Kane, D. L., & Hinzman, L. D. (1999). An analysis of an arctic channel network using a digital elevation model. Geomorphology, 29(3-4), 339-353.

Miralles, D. G., Holmes, T. R. H., De Jeu, R. A. M., Gash, J. H., Meesters, A. G. C. A., & Dolman, A. J. (2011). Global land-surface evaporation estimated from satellite-based observations. *Hydrology and Earth System Sciences, 15*(2), 453-469. doi:10.5194/hess-15-453-2011

Muskett, R. R., & Romanovsky, V. E. (2009). Groundwater storage changes in arctic permafrost watersheds from GRACE andin situmeasurements. *Environmental Research Letters, 4*(4). doi:10.1088/1748-9326/4/4/045009

Muskett, R. R., & Romanovsky, V. E. (2011). Energy and mass changes of the Eurasian permafrost regions by multi-satellite and in-situ measurements. *Natural Science, 03*(10), 827-836. doi:10.4236/ns.2011.310108

Neilson, B. T., Cardenas, M. B., O'Connor, M. T., Rasmussen, M. T., King, T. V., & Kling, G. W. (2018). Groundwater Flow and Exchange Across the Land Surface Explain Carbon Export Patterns in Continuous Permafrost Watersheds. *Geophysical Research Letters, 45*(15), 7596-7605. doi:10.1029/2018gl078140

O'Brien, W. J., Barfield, M., & Sigler, K. (2001). The functional response of drift-feeding Arctic grayling: the effects of prey density, water velocity, and location efficiency. *Canadian Journal of Fisheries and Aquatic Sciences, 58*(10), 1957-1963. doi:10.1139/cjfas-58-10-1957

O'Connor, M. T., Cardenas, M. B., Ferencz, S. B., Wu, Y., Neilson, B. T., Chen, J., & Kling, G. W. (2020). Empirical Models for Predicting Water and Heat Flow Properties of Permafrost Soils. *Geophysical Research Letters, 47*(11). doi:10.1029/2020gl087646

Olefeldt, D., Goswami, S., Grosse, G., Hayes, D., Hugelius, G., Kuhry, P., McGuire, A.D., Romanovsky, V.E., Sannel, A.B.K., Schuur, E.A.G. and Turetsky, M.R (2016). Circumpolar distribution and carbon storage of thermokarst landscapes. *Nat Commun, 7*, 13043. doi:10.1038/ncomms13043

Osterkamp, T. E. (2007). Characteristics of the recent warming of permafrost in Alaska. *Journal of Geophysical Research, 112*(F2). doi:10.1029/2006jf000578

Osuch, M., & Wawrzyniak, T. (2017). Variations and changes in snow depth at meteorological stations Barentsburg and Hornsund (Spitsbergen). *Annals of Glaciology, 58*(75pt1), 11-20. doi:10.1017/aog.2017.20

Painter, S. L., Moulton, J. D., & Wilson, C. J. (2012). Modeling challenges for predicting hydrologic response to degrading permafrost. *Hydrogeology Journal, 21*(1), 221-224. doi:10.1007/s10040-012-0917-4

Painter, S.L., Moulton, J.D., Wilson, C.J., Atchley, A.L., Berndt, M., Coon, E., Gangodagamage, C., Garimella, R., Miller, T.A. and Short, L.S. (2013). Microtopography-resolving simulations of surface and subsurface hydrology in thawing and topographically evolving permafrost regions. AGUFM, 2013, C52A-05.

Park, H., Fedorov, A. N., Zheleznyak, M. N., Konstantinov, P. Y., & Walsh, J. E. (2014). Effect of snow cover on pan-Arctic permafrost thermal regimes. *Climate Dynamics, 44*(9-10), 2873-2895. doi:10.1007/s00382-014-2356-5

Pulliainen, J., Luojus, K., Derksen, C., Mudryk, L., Lemmetyinen, J., Salminen, M., Ikonen, J., Takala, M., Cohen, J., Smolander, T. and Norberg, J. (2020). Patterns and trends of Northern Hemisphere snow mass from 1980 to 2018. *Nature, 581*(7808), 294-298. doi:10.1038/s41586-020-2258-0

Quinton, W. L., & Marsh, P. (1998). The influence of mineral earth hummocks on subsurface drainage in the continuous permafrost zone. Permafrost and Periglacial Processes, 9(3), 213-228.

Rawlins, M. A., Serreze, M. C., Schroeder, R., Zhang, X., & McDonald, K. C. (2009). Diagnosis of the record discharge of Arctic-draining Eurasian rivers in 2007. *Environmental Research Letters, 4*(4). doi:10.1088/1748-9326/4/4/045011

Rodell, M., & Famiglietti, J. S. (1999). Detectability of variations in continental water storage from satellite observations of the time dependent gravity field. *Water Resources Research, 35*(9), 2705-2723. doi:10.1029/1999wr900141

Romanovsky, V. E., & Osterkamp, T. E. (1997). Thawing of the active layer on the coastal plain of the Alaskan Arctic. Permafrost and Periglacial processes, 8(1), 1-22.

Rushlow, C. R., & Godsey, S. E. (2017). Rainfall-runoff responses on Arctic hillslopes underlain by continuous permafrost, North Slope, Alaska, USA. *Hydrological Processes, 31*(23), 4092-4106. doi:10.1002/hyp.11294

Schaefer, K., Zhang, T., Bruhwiler, L., & Barrett, A. P. (2011). Amount and timing of permafrost carbon release in response to climate warming. *Tellus B, 63*(2), 165-180. doi:10.1111/j.1600-0889.2011.00527.x

Scheidegger, J. M. (2013). Impact of permafrost dynamics on Arctic groundwater ow systems with application to the evolution of spring and lake taliks (Doctoral dissertation, University of East Anglia).

Schuur, E.A., Bockheim, J., Canadell, J.G., Euskirchen, E., Field, C.B., Goryachkin, S.V., Hagemann, S., Kuhry, P., Lafleur, P.M., Lee, H. and Mazhitova, G. (2008). Vulnerability of permafrost carbon to climate change: Implications for the global carbon cycle. BioScience, 58(8), 701-714.

St. Jacques, J.-M., & Sauchyn, D. J. (2009). Increasing winter baseflow and mean annual streamflow from possible permafrost thawing in the Northwest Territories, Canada. *Geophysical Research Letters, 36*(1). doi:10.1029/2008gl035822

Stieglitz, M., Déry, S. J., Romanovsky, V. E., & Osterkamp, T. E. (2003). The role of snow cover in the warming of arctic permafrost. *Geophysical Research Letters, 30*(13). doi:10.1029/2003gl017337

Sturm, M., Holmgren, J., & Liston, G. E. (1995). A seasonal snow cover classification system for local to global applications. Journal of Climate, 8(5), 1261-1283.

Swenson, S. C., Lawrence, D. M., & Lee, H. (2012). Improved simulation of the terrestrial hydrological cycle in permafrost regions by the Community Land Model. *Journal of Advances in Modeling Earth Systems, 4*(3), n/a-n/a. doi:10.1029/2012ms000165

Syvitski, J. P. (2002). Sediment discharge variability in Arctic rivers: implications for a warmer future. Polar Research, 21(2), 323-330.

Treat, C. C., & Jones, M. C. (2018). Near-surface permafrost aggradation in Northern Hemisphere peatlands shows regional and global trends during the past 6000 years. *The Holocene, 28*(6), 998-1010. doi:10.1177/0959683617752858

Velicogna, I., Tong, J., Zhang, T., & Kimball, J. S. (2012). Increasing subsurface water storage in discontinuous permafrost areas of the Lena River basin, Eurasia, detected from GRACE. *Geophysical Research Letters, 39*(9), n/a-n/a. doi:10.1029/2012gl051623

Vey, S., Steffen, H., Müller, J., & Boike, J. (2012). Inter-annual water mass variations from GRACE in central Siberia. *Journal of Geodesy, 87*(3), 287-299. doi:10.1007/s00190-012-0597-9

Walvoord, M. A., & Kurylyk, B. L. (2016). Hydrologic Impacts of Thawing Permafrost-A Review. *Vadose Zone Journal, 15*(6). doi:10.2136/vzj2016.01.0010

Walvoord, M. A., Voss, C. I., & Wellman, T. P. (2012). Influence of permafrost distribution on groundwater flow in the context of climate-driven permafrost thaw: Example from Yukon Flats Basin, Alaska, United States. *Water Resources Research, 48*(7). doi:10.1029/2011wr011595

Wang, H., Xiang, L., Jia, L., Wu, P., Steffen, H., Jiang, L., & Shen, Q. (2015). Water storage changes in North America retrieved from GRACE gravity and GPS data. *Geodesy and Geodynamics*, *6*(4), 267-273. doi:10.1016/j.geog.2015.07.002

Wang, W., Rinke, A., Moore, J.C., Ji, D., Cui, X., Peng, S., Lawrence, D.M., McGuire, A.D., Burke, E.J., Chen, X. and Decharme, B. (2016). Evaluation of air–soil temperature relationships simulated by land surface models during winter across the permafrost region. *The Cryosphere*, *10*(4), 1721-1737. doi:10.5194/tc-10-1721-2016

Watkins, M. M., D. N. Wiese, D.-N. Yuan, C. Boening, and F. W. Landerer (2015), Improved methods for observing Earth's time variable mass distribution with GRACE using spherical cap mascons, J. Geophys. Res. Solid Earth, 120, doi:10.1002/2014JB011547.

Wiese, D. N., Landerer, F. W., & Watkins, M. M. (2016). Quantifying and reducing leakage errors in the JPL RL05M GRACE mascon solution. *Water Resources Research*, *52*(9), 7490-7502. doi:10.1002/2016wr019344

Wiese, D. N., D.-N. Yuan, C. Boening, F. W. Landerer, M. M. Watkins. (2018). JPL GRACE Mascon Ocean, Ice, and Hydrology Equivalent Water Height Release 06 Coastal Resolution Improvement (CRI) Filtered Version 1.0. Ver. 1.0. PO.DAAC, CA, USA. Dataset accessed [2020-01-15] at http://dx.doi.org/10.5067/TEMSC-3MJC6.

Woo, M. K., & Guan, X. J. (2006). Hydrological connectivity and seasonal storage change of tundra ponds in a polar oasis environment, Canadian High Arctic. Permafrost and Periglacial Processes, 17(4), 309-323.

Peng, X., Zhang, T., Frauenfeld, O.W., Wang, K., Luo, D., Cao, B., Su, H., Jin, H. and Wu, Q., (2018). Spatiotemporal Changes in Active Layer Thickness under Contemporary and Projected Climate in the Northern Hemisphere. *Journal of Climate*, *31*(1), 251-266. doi:10.1175/jcli-d-16-0721.1

Zhang, T. (2005). Spatial and temporal variability in active layer thickness over the Russian Arctic drainage basin. *Journal of Geophysical Research*, *110*(D16). doi:10.1029/2004jd005642

Zhang, Y., Chen, W., & Riseborough, D. W. (2008). Disequilibrium response of permafrost thaw to climate warming in Canada over 1850–2100. *Geophysical Research Letters*, *35*(2). doi:10.1029/2007gl032117

Zhong, X., Zhang, T., Kang, S., Wang, K., Zheng, L., Hu, Y., & Wang, H. (2018). Spatiotemporal variability of snow depth across the Eurasian continent from 1966 to 2012. *The Cryosphere*, *12*(1), 227-245. doi:10.5194/tc-12-227-2018

Zimov, S. A., Schuur, E. A., & Chapin III, F. S. (2006). Permafrost and the global carbon budget. Science(Washington), 312(5780), 1612-1613.